An Indoor Localization and Tracking System Using Successive Weighted RSS Projection

K. Wen, C. K. Seow, *Senior Member, IEEE* and S.Y. Tan, *Member, IEEE*

***Abstract*—This letter proposes a novel successive weighted received signal strength (RSS) indoor localization and tracking system that projects previous time instance estimated mobile device (MD) position to provide projected RSS values. Such RSS projection increases the number of available RSS from N_m to $N_m + N_{AP}$, where N_{AP} is the total number of access points and N_m is the number of RSS values measured by MD, ranging from 0 to N_{AP}. Our proposed system thus resolves the issues associated with insufficient or no RSS values received by MD. Inertial navigation system (INS) is merged with RSS localization system to provide a weighted fusion of projected and measured RSS values. The weighting factors are derived based on the INS and RSS localization accuracy where the former is initially accurate but deteriorates with time and the latter is time-independent but environment-dependent. The proposed system was tested in indoor environments and outperformed other existing localization systems such as RSS and INS fusion using extended Kalman filter and non-line-of-sight selection scheme, especially in heavy multipath environment, by 42% and 75%, respectively.**

***Index Terms*— indoor localization and tracking, received signal strength, strapdown inertial navigation system.**

I. Introduction

Indoor localization and tracking systems are rapidly developing due to an increasing number of available sensors. A variety of wireless infrastructure presently exist, including wireless local area network (WLAN), radio-frequency identification (RFID), and ultra-wideband (UWB) [1]-[3]. Information often required for localization include time of arrival (TOA), angle of arrival (AOA), and received signal strength (RSS) [4]-[8]. RSS systems offer advantages over other systems, such as low implementation costs and simple measurement acquisition. RSS can be used to compute ranges either through signal propagation models [9] or by constructing a fingerprinting database [10], the latter of which involves a particularly labor-extensive training process, which may not always be feasible. RSS system using the propagation approach is cost-effective, practical, and has statistically time-independent localization performance. However, localization accuracy is affected by the accuracy of the propagation model parameters used in complex indoor environments [11]. Insufficient or sometimes absent RSS measurements are another hindrance that degrades localization performance. Such issues can be mitigated by cooperating with other systems. For example, inertial navigation system (INS) is readily available for handheld devices and uses measurements from inertial measuring units (IMU), which normally includes accelerometers and gyroscopes. Strapdown INS pedestrian dead reckoning (PDR) transforms tri-axial accelerations and angular velocity measurements from the IMU body frame to the global navigation frame before integration to track a user's location and orientation [12]. The propagation of measurement errors through coordinate transformation and integration causes accumulation of localization and orientation errors despite it is accurate during the initial movement stage [13]. Hence INS has time-dependent localization performance.

Current research is focusing on the fusion of INS and RSS using Bayesian filters. Zero velocity updating (ZUPT) using extended Kalman filter (EKF) has been applied as a recalibration method [14], and particle filter (PF) together with a layout map has been used to model nonlinear systems [15]. The EKF scheme requires accurate real-time covariance values, which are difficult to obtain, and the PF scheme relies heavily on map constraints, which is challenging to implement in cases of inaccurate mapping or in environments with scarce physical constraints. In this letter, we propose a novel successive weighted RSS localization and tracking system fused with strapdown INS PDR to increase the number of available RSS values from N_m to $N_m + N_{AP}$, where N_{AP} is the total number of access points (APs) and N_m is the number of RSS values measured by a mobile device (MD), ranging from 0 to N_{AP}. It resolves the issue of insufficient RSS measurements for localization, especially in heavy multipath environments. Furthermore, time-dependent weighting factors are derived on the basis of accuracy characteristics of RSS system and INS. To the best of our knowledge, no reported literature has proposed successive RSS projection with time-dependent weighting factors for indoor localization and tracking. This letter is organized as follows. The proposed fusion system is described in section II, followed by a presentation of the experimental results and comparison with other fused systems in section III, and conclusion in section IV.

II. Proposed Successive Weighted RSS System

The RSS localization accuracy suffers when insufficient RSS measurements occur. INS projection from previously estimated location at t_{i-1} is used to provide additional projected RSS values at t_i. The measured and projected RSS values are weighted and linearly combined to obtain the fused RSS values. The weighting factors are time-dependent and derived based on the relative accuracy of measured and projected RSS values at t_i. The fused RSS values are used to obtain the estimated

location at t_i which complete the successive weighted RSS localization and tracking system.

A three-dimensional IMU measures the tri-axial angular velocity and specific force at t_i, which can be expressed as $\boldsymbol{\omega}^b_{xyz,i} = \left[\omega^b_{x,i}, \omega^b_{y,i}, \omega^b_{z,i}\right]^T$ and $\mathbf{f}^b_{xyz,i} = \left[f^b_{x,i}, f^b_{y,i}, f^b_{z,i}\right]^T$, where the superscript b indicates the body frame. The accelerations are mapped to navigation frame N using transformation matrix $\mathbf{C}^N_b$, whose change rate $\dot{\mathbf{C}}^N_b$ can be formulated as $\dot{\mathbf{C}}^N_{b,i} = \mathbf{C}^N_{b,i}\boldsymbol{\Omega}$ where $\boldsymbol{\Omega}$ is a matrix with its rows expressed as $\boldsymbol{\Omega}_{1,1\ldots3} = \left[0, -\omega^b_{z,i}, \omega^b_{y,i}\right]$, $\boldsymbol{\Omega}_{2,1\ldots3} = \left[\omega^b_{z,i}, 0, -\omega^b_{x,i}\right]$ and $\boldsymbol{\Omega}_{3,1\ldots3} = \left[-\omega^b_{y,i}, \omega^b_{x,i}, 0\right]$ [16]. Gyroscope and accelerometer measurements are used to form the attitude estimator to estimate $\boldsymbol{\omega}^b_{xyz,i}$ biases and improve $\mathbf{C}^N_b$ estimation. When the IMU is stationary or moving at a constant speed, the attitude estimator that uses the relationship between G and $\mathbf{f}^b_{xyz,i}$ is formulated as $\mathbf{f}^b_{xyz,i} = (\mathbf{C}^N_{b,i})^T[0, 0, G]^T$ where G is the gravitational acceleration. The third row of $\mathbf{C}^N_b$ and $\boldsymbol{\omega}^b_{xyz,i}$ biases form the adaptive EKF states, which use the formulation of $\dot{\mathbf{C}}^N_b$ and $\mathbf{f}^b_{xyz,i}$ as propagation and measurement stage models, respectively [16]. Magnetometer can also be incorporated to further improve the heading estimation [17]. The navigation frame acceleration is calculated as $\mathbf{a}^N_{xyz,i} = \mathbf{C}^N_{b,i}\,\mathbf{f}^b_{xyz,i} - [0, 0, G]^T$. Its navigation frame velocity $\mathbf{v}^N_{XYZ,i}$ and location $\mathbf{p}^N_{XYZ,i}$ can be obtained using single and double integration of $\mathbf{a}^N_{XYZ,i}$, respectively. The INS-calculated location propagates the MD into its projected location and the standard deviation of the localization error σ^{INS}_i is tracked. Instantaneous variances of $\mathbf{a}^N_{XYZ}$, $Var(\mathbf{a}^N_{XYZ,i})$ are formulated by substituting the variances of gaussian noise in IMU measurements $\boldsymbol{\omega}^b_{xyz,i}$ and $\mathbf{f}^b_{xyz,i}$ which are acquired using Allan variance technique into the formulation of $\mathbf{a}^N_{XYZ,i}$. The details can be found in our previous paper [13]. The $Var(\mathbf{a}^N_{XYZ,i})$ are integrated to find velocity variances $Var(\mathbf{v}^N_{XYZ,i})$ and position variances $Var(\mathbf{p}^N_{XYZ,i})$.The $(\sigma^{INS}_i)^2$ is expressed as $Var(p^N_{X,i}) + Var(p^N_{Y,i}) + Var(p^N_{Z,i})$, which grows over time due to the accumulation of $Var(\mathbf{a}^N_{XYZ,0\ldots i})$. Both projected location and σ^{INS}_i are used to form the successive weighted RSS system.

The above-mentioned INS projection is illustrated in Fig. 1 where the ground truth path and true MD locations at t_{i-1} and t_i are depicted. The distance from k^{th} AP (AP$_k$) to the true MD location at t_i is denoted as $d^o_{i,k}$ where $k = 1\ldots N_{AP}$ where N_{AP} is total number of APs. Three INS projection scenarios with different accuracies are represented by $\sigma^{INS,S=1,2,3}_i$ where $\sigma^{INS,1}_i \ll \sigma^{INS,2}_i \ll \sigma^{INS,3}_i$ and three loci of the estimated MD using measured RSS at t_i are shown. The estimated path using only INS for scenario 2 is also provided whereas scenario 1 and 3 are omitted for brevity. Estimated locations at t_{i-1} are projected to their locations at t_i based on the INS calculation. Two sets of distances are now available: the first distance set $d^{INS,S}_{i,k}$ is calculated from AP$_k$ to the projected MD location at t_i and the second distance set $d^{RSS,S}_{i,k}$ is based on RSS measurement from AP$_k$. The $d^o_{i,k}$ can be estimated using $w^{INS,S}_{i,k} d^{INS,S}_{i,k} + w^{RSS,S}_{i,k} d^{RSS,S}_{i,k}$

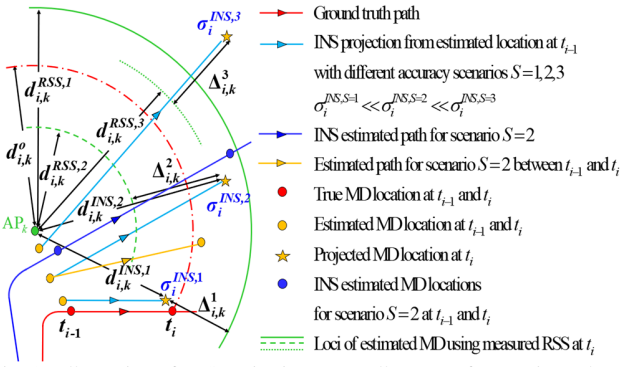

Fig. 1. Illustration of INS projection at t_i (yellow star) from estimated MD location at t_{i-1} (yellow circle) under different INS accuracy scenarios.

where $w^{INS,S}_{i,k}$ and $w^{RSS,S}_{i,k}$ are weighting factors. When INS is accurate (scenario 1), $w^{INS,1}_{i,k}$ should be much larger than $w^{RSS,1}_{i,k}$. When INS is less accurate (scenario 2), $w^{INS,2}_{i,k}$ should be smaller than $w^{INS,1}_{i,k}$ while $w^{RSS,2}_{i,k}$ is larger than $w^{RSS,1}_{i,k}$. When INS is not accurate (scenario 3), $w^{RSS,3}_{i,k}$ should be much larger than $w^{INS,3}_{i,k}$. Thus, the weighting factors are designed as

$$w^{INS,S}_{i,k} = \Delta^S_{i,k} / (\Delta^S_{i,k} + \sigma^{INS,S}_i),\ w^{RSS,S}_{i,k} = 1 - w^{INS,S}_{i,k} \qquad (1)$$

where $\Delta^S_{i,k} = \left| d^{RSS,S}_{i,k} - d^{INS,S}_{i,k} \right|$. Assuming $\sigma^{INS,1}_i \ll \Delta^1_{i,k}$ in scenario 1, $w^{INS,1}_{i,k} \approx 1$ and $w^{RSS,1}_{i,k} \approx 0$, which indicates that the estimated distance relies on the INS projection. Assuming $\sigma^{INS,2}_i = \Delta^2_{i,k}$ in scenario 2, $w^{INS,2}_{i,k} = w^{RSS,2}_{i,k} = 0.5$, which means that the INS projection and RSS measurement carry equal weight of the distance estimation. Assuming $\sigma^{INS,3}_i \gg \Delta^3_{i,k}$ in scenario 3, $w^{RSS,3}_{i,k} \approx 1$ and $w^{INS,3}_{i,k} \approx 0$, which indicates that the estimated distance relies on the RSS measurement. The estimated MD location at t_i is obtained using the weighted distance estimations from all APs. As shown in Fig. 1, the estimated MD location at t_i (yellow circle) using all APs is closer to true location (red circle) as compared to projected MD location (yellow star) for scenario 2.

A detailed implementation is given as follows. The initial MD and AP locations are assumed to be known with the measured RSS value at t_i from AP$_k$ expressed as

$$RSS^m_{i,k} = RSS_r - 10n\log_{10}\left(d^o_{i,k} / d_r\right) + \upsilon \qquad (2)$$

where RSS_r is the mean RSS at reference distance d_r, $d^o_{i,k}$ is the distance between the true MD location and AP$_k$, n is the path-loss exponent, and υ is used to account for the shadowing effect, which is modeled as a Gaussian random variable with standard deviation σ_υ [18], [19]. The maximum likelihood estimation of distance $d^{RSS}_{i,k}$, can be expressed as $d_r 10^{(RSS_r - RSS^m_{i,k})/(10n)}$. In Fig. 1, the RSS difference between the estimated MD location at t_{i-1} and its projected location at t_i is computed using (2) as $\Delta RSS_{i,k} = -10n\log_{10}(d^{INS}_{i,k}/d'_{i-1,k})$ where $d'_{i-1,k}$ and $d^{INS}_{i,k}$ are the distances from AP$_k$ to the estimated MD

location at t_{i-1} and its projected location at t_i using INS projection, respectively, independent of RSS at t_i. Hence the projected RSS at t_i, $RSS^{p}_{i,k}$ can be expressed as $RSS_{i-1,k} + \Delta RSS_{i,k}$ where $RSS_{i-1,k}$ is the fused RSS value at t_{i-1}. The fused RSS value at t_i is then obtained by combining the projected and measured RSS values using weighting factors as

$$RSS_{i,k} = w^{INS}_{i,k} RSS^{p}_{i,k} + w^{RSS}_{i,k} RSS^{m}_{i,k} \quad (3)$$

where $w^{INS}_{i,k}$ and $w^{RSS}_{i,k}$ are the weighting factors explained in (1). The estimated distance $d_{i,k}$ is then expressed as $d_r 10^{(RSS_r - RSS_{i,k})/(10n)}$. The estimated MD location $(\hat{X}_i, \hat{Y}_i)$ can be obtained using the weighted least square (LS) as

$$(\hat{X}_i, \hat{Y}_i) = \arg\min_{(X_i, Y_i)} \sum_{k=1}^{N_{AP}} \left\{ w_{i,k} \left[\sqrt{(X_i - X_{AP,k})^2 + (Y_i - Y_{AP,k})^2} - d_{i,k} \right] \right\}^2 \quad (4)$$

where $(X_{AP,k}, Y_{AP,k})$ represent AP_k coordinates, and $w_{i,k} = 1/d_{i,k}$ which is equivalent to $1/\sigma_{d_{i,k}}$ where $\sigma_{d_{i,k}}$ is the standard deviation of $d_{i,k}$ since $\sigma_{d_{i,k}} = d_{i,k}\sigma_v \ln(10)/(-10n)$ [14]. Assuming N_m is the number of APs with measurable RSS values ($N_m \leq N_{AP}$), N_m measured RSS values are used to fuse with N_{AP} projected RSS values to form $RSS_{i,k=1\ldots N_{AP}}$. The N_{AP} projected RSS values are obtained using INS projection from estimated MD location at t_{i-1}. Thus, the RSS projection increases the number of available RSS values from N_m to $N_m + N_{AP}$. Our proposed system resolves the issue where insufficient or no RSS values are received by the MD. Equations (3) and (4) form a recursive tracking system.

To further reduce time-dependent error, the weighting factor in (4) is extended to account for unmeasurable RSS value by introducing a scaling term $w'_{i,k}$ as outlined by cases 2-4 in Table I. When the MD fails to measure RSS from AP_k at t_i in case 2, less weight should be placed on the fused RSS as it is solely based on the projection. The $(w^{INS}_{i-L,k})^L$ term is introduced to further account for projection deterioration when RSS measurement remains absent in case 3 where L is the number of consecutive times that RSS is not measured. In case 4 when MD measures RSS value from previously unmeasurable AP_k, $w'_{i,k}$ equals to $\max\{ (w^{INS}_{i-L,k})^L, w^{RSS}_{i,k} \}$ by considering the relative weight of successive projections and RSS measurement. The weighting factor in (4) for AP_k becomes $w_{i,k} w'_{i,k}$.

III. Experimental Results and Discussion

An experimental campaign was conducted in an indoor environment of level B2 at the School of Electrical and Electronic Engineering, Nanyang Technological University, Singapore. Fig. 2 shows a panorama view of the 40 m × 100 m experimental layout covered by 14 APs. The environment is an office environment featuring numbers of meeting rooms, hallways, and pillars. All APs are Alcatel-Lucent Enterprise OmniAccess OAW-AP225 IEEE 802.11ac wireless access points. Sony XZ Premium smartphone and Xsens Mtw were used as the MD and IMU, whose sampling frequencies are 1 Hz and 100 Hz, respectively. Fusion is done at every second. In this

TABLE I
Modified Weight under Different RSS Cases at t_{i-1} and t_i

Case	$RSS^{m}_{i-1,k}$	$RSS^{m}_{i,k}$	$RSS_{i,k}$ in (3)	Weight $w'_{i,k}$
1	✓	✓	$w^{INS}_{i,k} RSS^{p}_{i,k} + w^{RSS}_{i,k} RSS^{m}_{i,k}$	1
2	✓	×	$RSS^{p}_{i,k}$	$w^{INS}_{i-1,k}$
3	×	×	$RSS^{p}_{i,k}$	$\left(w^{INS}_{i-L,k}\right)^L$
4	×	✓	$w^{INS}_{i,k} RSS^{p}_{i,k} + w^{RSS}_{i,k} RSS^{m}_{i,k}$	$\max\{\left(w^{INS}_{i-L,k}\right)^L, w^{RSS}_{i,k}\}$

✓ = RSS measured, × = RSS not measured.

experimental environment, the average reference RSS value for all APs was found to be -53 dBm. The n was estimated by collecting measurements from 280 scattered locations with known coordinates. The distances d between those locations and 14 APs range from 7.4 m to 73.4 m. The relationship between $RSS_r - RSS^m$ and $10\log_{10}(d)$ are fitted using linear regression and n was found to be 2.34, which is similar to 2.3 reported in [14]. Walking routes 1 and 2 displayed in Fig. 2 are in relatively open and heavily blocked region, respectively. The ground truth paths are labeled by markers at every meter point for reference. Magnetometers measurements were omitted in this study because the magnetic field strength measurements fluctuated between 16.8 A/m and 63.8 A/m in this environment, whereas the value measured in an outdoor open field was 34.3 A/m. EKF scheme is included for localization performance comparison. Reference [14] proposed a tight-coupling fusion system that uses the calculated range from RFIDs to the INS location and the estimated range using a path-loss model at the current time as measurements. The σ_v is required for EKF and was set to 6 dB in [14]. It is found that EKF performance is insensitive to σ_v, varying from 3 to 9 dB in the experimental environment while 6 dB yields the smallest cumulative error. Hence 6 dB was used in our test. Another RSS with INS localization scheme [20] is added for comparison. Reference [20] applied user-specific step-length based PDR to provide preliminary localization as the first part of the system. The center point of the LS localization results from the four highest RSS values is used to replace the PDR localization if the non-line-of-sight (NLOS) signal is not detected.

Tracking trajectories from various schemes of both routes are shown in Fig. 3. Our proposed scheme with modified weighted

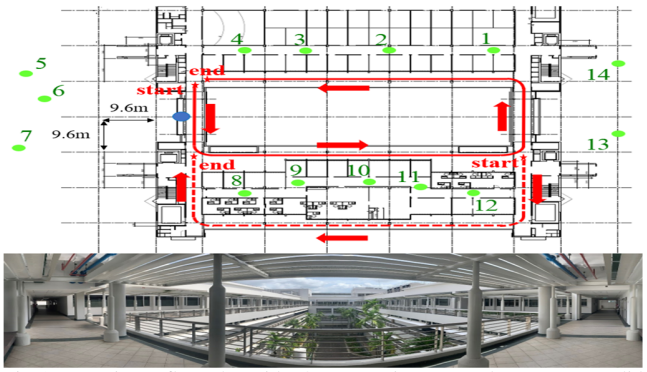

Fig. 2. Experiment floor plan with 14 access points (green dots), route 1 (solid red line), route 2 (dash red line), and the panorama view (from blue dot).

LS remains closer to the true paths during nearly the entire time. Fluctuations of the tracking path are mainly owing to an insufficient number of APs detected by the MD. An average of 9 and 5 RSS measurements were collected at each time instance for routes 1 and 2, respectively, reducing to 6 and 3 at route corners. Our proposed scheme increases the number of RSS to provide 14 fused RSS values at any time. For illustration at 10 s along route 1 (before first turn) in Fig. 2 when 9 RSS measurements were available, the INS provided accurate projected RSS values for all APs including 5 unavailable APs. Our proposed scheme using 14 fused RSS values yields 2.1 m localization error compared to 7.7 m from the one using 9 RSS values, which achieves 73% improvement. At 40 s (before second turn), only 7 RSS measurements were available. Our proposed scheme added additional 7 projected RSS values using methodology described in Table I. The additional RSS values reduces error from 12.4 m to 5.3 m (57% improvement) even with larger σ^{INS}. Another factor causing fluctuations is the poor distance estimation. This is a result of inaccurate RSS measurements owing to small scale fading caused by multipath signals. Recalibration on INS or adding more APs can be used to further contain fluctuations. Weighting factors w^{INS} and w^{RSS} together with σ^{INS} along route 1 are shown in Fig. 4. As given in (1), the weighting factor w^{INS} decreases over time, which indicates that the contribution of the projected RSS decreases due to deterioration of the INS projection. The w^{INS} reaches 0.5 at roughly 23 s and it drops to 0.4 around 40 s. To further enhance the proposed scheme, recalibration on IMU can be done through stationary or known IMU state when w^{INS} and w^{RSS} intersect which happens at 23 s. The w^{INS}, w^{RSS}, and σ^{INS} are reset to initial values after recalibration. The subsequent recalibrations happen at 48 s and 69 s. Fig. 5 depicts cumulative and absolute localization errors of the fusion schemes at every second for route 1. RSS stand-alone localization results using either LS or weighted LS are added for performance comparison. For route 1, the cumulative (and mean absolute) error at 84 s determined by the proposed scheme without recalibration, EKF, RSS with LS, RSS with weighted LS, and NLOS selection scheme are 348 (4.1) m, 490 (5.8) m, 635 (7.6) m, 469 (5.6) m, and 540 (6.4) m, respectively. Our proposed scheme shows a 29% and 36% performance advantage over EKF and NLOS selection scheme, respectively. Recalibration has reduced cumulative (and mean absolute) error from 348 (4.1) m to 217 (2.6) m, with a 38% improvement compared to

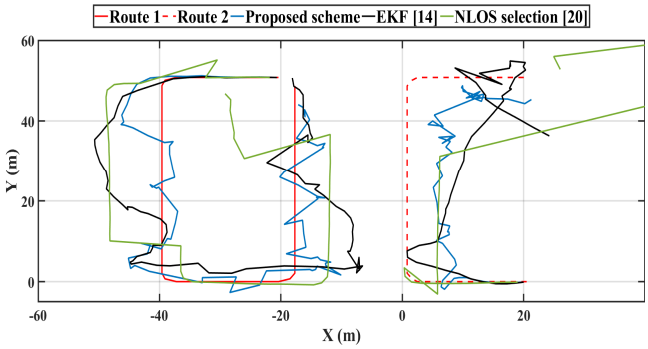

Fig. 3. Route 1 and route 2 tracking trajectories comparison.

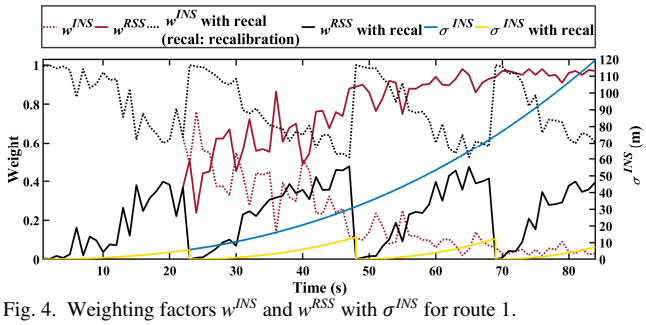

Fig. 4. Weighting factors w^{INS} and w^{RSS} with σ^{INS} for route 1.

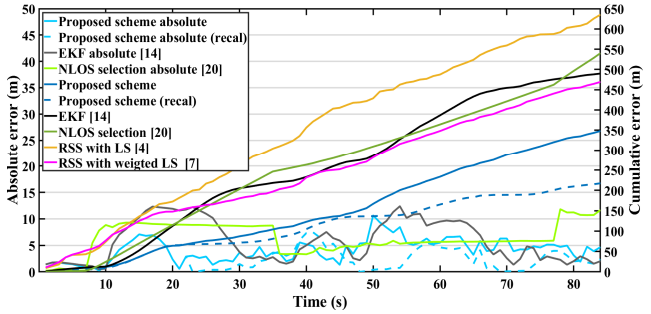

Fig. 5. Cumulative and absolute localization errors for route 1.

the proposed scheme without recalibration. Error plot for route 2 is omitted for brevity. For route 2, the cumulative error at 53 s are 328 m, 564 m, 619 m, 610 m, and 1305 m, respectively, yielding a 42% and 75% performance advantage of the proposed scheme without recalibration over EKF and NLOS selection scheme, respectively. Tests were also performed under other n to investigate the robustness of these schemes. Since n values typically fall within 2.0 to 4.0 in office environment [18], tests are also conducted when n = 2.0, 3.0, and 4.0. For route 1, our proposed scheme without recalibration has 32%, 20%, and 23% less cumulative error than EKF when n = 2.0, 3.0, and 4.0, respectively, and 43%, 34%, and 45% less cumulative error than the NLOS selection scheme. The cumulative error fluctuations are 134 m, 277 m, and 315 m for proposed scheme without recalibration, EKF, and NLOS selection scheme, respectively. Similar results are obtained for route 2. This verifies that the proposed scheme is more accurate and more robust than the other two fusion schemes.

IV. Conclusion

In this letter, we have proposed a novel weighted successive RSS localization and tracking system with strapdown INS PDR assistance. The RSS projection that increases the number of available RSS values is explained. This projection addresses the issue of insufficient RSS measurements for localization and tracking, which is useful for handling heavy multipath environments. The time-dependent weighting factors and σ^{INS} are elaborated and displayed. Experiments in relatively open and heavily blocked environments show that our proposed system is more robust with superior performance over other localization systems such as RSS and INS fusion using EKF and NLOS selection scheme by 29% (42%) and 36% (75%) in light (heavy) multipath environments, respectively.

REFERENCES

[1] C. Feng, W. S. A. Au, S. Valaee, and Z. Tan, "Received-signal-strength-based indoor positioning using compressive sensing," *IEEE Trans. Mobile Comput.*, vol. 11, no. 12, pp. 1983–1993, Dec. 2012.

[2] A. A. N. Shirehjini, A. Yassine, and S. Shirmohammadi, "An RFID based position and orientation measurement system for mobile objects in intelligent environments," *IEEE Trans. Instrum. Meas.*, vol. 61, no. 6, pp. 1664–1675, Jun. 2012.

[3] H. Soganci, S. Gezici, H. Poor, "Accurate positioning in ultra-wideband systems," *IEEE Wireless Communications*, vol. 18, no. 2, pp. 19-27, Apr. 2011.

[4] S. W. Chen, C. K. Seow, S. Y. Tan, "Virtual reference device-based NLOS localization in multipath environment," *IEEE Antennas and Wireless Propag. Lett.*, vol. 13, pp. 1409-1412, Jul. 2014.

[5] H. Zhang, C. K. Seow, S. Y. Tan, "Virtual reference device-based narrowband TOA localization using LOS and NLOS path," in *Proc. IEEE/ION Position Location and Navigation Symposium (PLANS'16)*, 2016, pp. 225-231.

[6] C. K. Seow, S. Y. Tan, "Non-line-of-sight localization in multipath environments," *IEEE Trans. Mobile Computing*, vol. 7, no. 5, pp. 647-660, May 2008.

[7] S. W. Chen, C. K. Seow, S. Y. Tan, "Elliptical lagrange-based NLOS tracking localization scheme," *IEEE Trans. Wireless Commun.*, vol. 15, pp. 3212-3225, May 2016.

[8] A. Coluccia, "Reduced-bias ml-based estimators with low complexity for self-calibrating RSS ranging," *IEEE Trans. Wireless Commun.*, vol. 12, no. 3, pp. 1220–1230, Mar. 2013.

[9] J. Yang, Y. Chen, "Indoor localization using improved rss-based lateration methods," *Proc. 28th IEEE Conf. Global Telecommunications GLOBECOM'09*, 2009.

[10] E. Martin, O. Vinyals, G. Friedland, and R. Bajcsy, "Precise indoor localization using smart phones," in *Proc. 18th ACM Int. Conf. Multimedia,* 2010, pp. 787–790.

[11] Q. Sun, S. Y. Tan, K. C. Teh, "Analytical formulae for path loss prediction in urban street grid microcellular environments," *IEEE Trans. Veh. Technol.*, vol. 54, no. 4, pp. 1251-1258, Jul. 2005.

[12] E. Foxlin, "Pedestrian tracking with shoe-mounted inertial sensors," *IEEE Comput. Graph. Appl.*, vol. 25, no. 6, pp. 38-46, Nov./Dec. 2005.

[13] K. Wen, C. K. Seow, S. Y. Tan, "Inertial navigation system positioning error analysis and Cramér-Rao lower bound, " in *Proc. IEEE/ION Position Location and Navigation Symposium (PLANS'16)*, 2016, pp. 213-218.

[14] A. R. J. Ruis, F. S. Granja, J. C. P. Honorato, J. I. G. Rosas, "Accurate pedestrian indoor navigation by tightly coupling foot-mounted IMU and RFID measurements," *IEEE Trans. Instrum. Meas.*, vol. 61, no. 1, pp. 178-189, Jan. 2012.

[15] F. Seco, A. R. Jiménez, "Smartphone-based cooperative indoor localization with RFID technology," *Sensors*, vol. 18, no. 1, pp. 266, Jan. 2018.

[16] H. Hyyti, A. Visala, "A DCM based attitude estimation algorithm for low-cost MEMS IMUs," *Int. J. Navig. Obs.*, pp. 18, Nov. 2015.

[17] W. Li, J. Wang, "Effective adaptive Kalman filter for MEMS-IMU/magnetometers integrated attitude and heading reference systems", *J. Navigat.*, vol. 66, no. 1, pp. 99-113, Jan. 2013.

[18] S. Y. Seidel, T. S. Rappaport, "914 MHz path loss prediction models for indoor wireless communications in multifloored buildings", *IEEE Trans. Antennas Propagat.*, vol. 40, pp. 207-217, Feb. 1992.

[19] S. Mazuelas, A. Bahillo, R. M. Lorenzo, P. Fernandez, F. A. Lago, E. Garcia, J. Blas, E. J. Abril, "Robust indoor positioning provided by real-time RSSI values in unmodified WLAN networks," *IEEE J. Sel. Topics Signal Process.*, vol. 3, no. 5, pp. 821-831, Oct. 2009.

[20] H. Cho, Y. Kwon, "RSS-based indoor localization with PDR location tracking for wireless sensor networks," *AEU-Int. J. Electron. Commun.*, vol. 70, no. 3, pp. 250-256, Mar. 2016.